pressure across the array relaxes to zero there is a clearly distinguishable tone smoothly drifting from high to low frequency during the transient, which lasts for several seconds. This simple observation marks the discovery of coherent quantum oscillations between weakly coupled superfluids.

To quantify this assertion we have processed several digitally recorded transient signals. Each transient is broken into equal, short time intervals. The average membrane position during the interval is used to calculate the pressure difference. For each time interval we compute the power spectrum of the membrane motion. As the frequency is drifting during any interval, the peak in the Fourier transform is not sharp. We identify the centre frequency of the strongest spectral component in the range of interest. This is the oscillation frequency corresponding to the pressure difference across the weak link during that interval.

Figure 2 plots the oscillation frequency, f, as a function of ΔP for a series of different temperatures. The frequency is found to be proportional to ΔP, the proportionality factor being 194 kHz Pa^{-1}, with a statistical error of ± 1 kHz Pa^{-1}, and a systematic uncertainty of ± 15 kHz Pa^{-1}. The linear relationship between f and ΔP, and the measured value of the slope, are in clear agreement with equation (3), over a pressure range of more than two orders of magnitude. This is a direct confirmation of the quantum-oscillation equation for superfluid ^{3}He.

The relation between frequency and pressure difference is observed to be independent of temperature, to within the error of the measurement. It is expected[13,14,17] that the actual current–phase relation might become increasingly distorted from the simple sine form in equation (1) as the coherence length gets smaller with falling temperature[7]. The distorted $I(\Delta\phi)$ would lead to higher harmonics of the quantum oscillations. We have searched for these higher harmonics in the spectral signal of the sound, and find that (to within our signal-to-noise ratio) they are absent over a wide range of temperatures.

The experimental results reported here lead to three significant conclusions. (1) The aperture array behaves like a single coherent superfluid weak link. (2) The current–phase relation is similar to the d.c. Josephson equation (equation (1)), that is periodic with modulus 2π. (3) The time evolution of the quantum phase across the array leads to current oscillations that drive the upper diaphragm at the frequency predicted by equation (3).

The remarkable properties of the weak-link array may lead to the observation of several physical phenomena analogous to those found in superconductivity. These include Shapiro[23] steps and, perhaps most significantly, the development of the superfluid analogue of a d.c. SQUID[24]. □

Received 5 June; accepted 30 June 1997.

1. Josephson, B. D. Possible new effects in superconductive tunneling. Thesis, Cambridge Univ. (1962).
2. Anderson, P. W. in *Lectures on the Many-Body Problem* (ed. Caianello, E. R.) 113–135 (Academic, New York, 1964).
3. Feynman, R. P. *The Feynman Lectures on Physics* Sect. 21-9 (Addison Wesley, New York, 1965).
4. Josephson, B. D. Possible new effects in superconductive tunnelling. *Phys. Lett.* **1,** 251–253 (1962).
5. Reif, F. *Fundamentals of Statistical and Thermal Physics* Sect. 8-7 (McGraw-Hill, New York, 1965).
6. Tilley, D. R. & Tilley, J. *Superfluidity and Superconductivity* (Hilger, New York, 1990).
7. Vollhardt, D. & Woolfle, P. *The Superfluid Phases of Helium-3* Sect. 7-2 (Taylor & Francis, New York, 1990).
8. Tilley, D. R. & Tilley, J. *Superfluidity and Superconductivity* Sect. 7-6 (Hilger, New York, 1990).
9. Pereverzev, S. V. Toward the Josephson effect in superfluid helium: how to make 20 nm holes in a 10 nm thick membrane. *J. Low Temp. Phys.* **101,** 573–579 (1995).
10. Amar, A., Sasaki, Y., Lozes, R. L., Davis, J. C. & Packard, R. E. Fabrication of submicron apertures in thin membranes of silicon nitride. *J. Vac. Sci. Technol. B* **11,** 259–262 (1993).
11. Paik, H. J. Superconducting tunable-diaphragm transducer for sensitive acceleration measurements *J. Appl. Phys.* **47,** 1168–1178 (1976).
12. Avenel, O. & Varoquaux, E. in *Proc. 10th Int. Cryogenic Eng. Conf.* (eds Klipping, G. & Klipping, I.) 587–589 (Butterworths, Guildford, 1986).
13. Monien, H. & Tewordt, L. Theory of Josephson flow oscillations in superfluid ^{3}He-B. *J. Low Temp. Phys.* **62,** 277–300 (1986).
14. Hook, J. R. Current-phase relation for flow of an *s*-wave paired superfluid through a cylindrical channel of finite length. *Jpn. J. Appl. Phys.* **26,** 159–160 (1987).
15. Kurkijärvi, J. Josephson current through a short and narrow orifice in a p-wave superfluid. *Phys. Rev. B* **38,** 11184–11187 (1988).
16. Thuneberg, E. V. Two dimensional simulation of the Josephson Effect in superfluid ^{3}He. *Europhys. Lett.* **7,** 441–446 (1988).
17. Ullah, S. & Fetter, A. L. Superfluid ^{3}He-B in a weak link. *Phys. Rev. B* **39,** 4186–4190 (1989).
18. Thuneberg, E. V., Kurkijärvi, J. & Sauls, J. A. Quasiclassical theory of the Josephson effect in superfluid ^{3}He. *Physica B* **165&166,** 755–756 (1990).
19. Avenel, O. & Varoquaux, E. Josephson effect and quantum phase slippage in superfluids. *Phys. Rev. Lett.* **60,** 416–419 (1988).
20. Varoquaux, E., Avenel, O., Ihas, G. & Salmelin, R. Phase slippage in superfluid ^{3}He-B. *Physica B* **178,** 309–316 (1990).
21. Steinhauer, J. The current-pressure relation for a superfluid ^{3}He weak link. Thesis, Univ. California, Berkeley (1995).
22. Mukharsky, Yu. M., Loshak, A., Schwab, K., Davis, J. C. & Packard, R. E. Study of an array of superfluid ^{3}He weak links. *Czech. J. Phys.* **46,** 115–116 (1996).
23. Shapiro, S. Josephson currents in superconducting tunnelling; the effect of microwaves and other observations. *Phys. Rev. Lett.* **11,** 80–82 (1963).
24. Packard, R. E. & Vitale, S. Principles of superfluid-helium gyroscopes. *Phys. Rev. B* **46,** 3540–3549 (1992).

Acknowledgements. In early stages of this work we were helped by J. Steinhauer, K. Schwab, Yu. M. Murkarsky and I. Schuster. E. W. Hudson made important contributions to the data acquisition system. Figure 1b was made by R. Orr. The aperture array was constructed at the Berkeley Microfabrication Laboratory. This work was supported in part by the National Science Foundation, the Office of Naval Research, and the Packard Foundation.

Correspondence and requests for materials should be addressed to R.E.P. (e-mail: packard@socrates.berkeley.edu).

Graphitic cones and the nucleation of curved carbon surfaces

A. Krishnan*, E. Dujardin†, M. M. J. Treacy*, J. Hugdahl‡, S. Lynum‡ & T. W. Ebbesen*§

** NEC Research Institute, 4 Independence Way, Princeton, New Jersey 08540, USA*
† Laboratoire de Chimie, Collège de France, 11, place M. Berthelot, 75005 Paris, France
‡ Kvaerner Engineering a.s., 1324 Lysaker, Norway
§ ISIS, Louis Pasteur University, rue Blaise Pascal, 67000 Strasbourg, France

The nucleation and growth of curved carbon structures, such as fullerenes, nanotubes and soot, are still not well understood. A variety of models have been proposed[1–17], and it seems clear that the occurrence of pentagons, which yield 60° disclination defects in the hexagonal graphitic network, is a key element in the puzzle. The problem of nucleation has been complicated by the great variety of structures observed in any one sample. Here we report an unusual carbon sample generated by pyrolysis of hydrocarbons, consisting entirely of graphitic microstructures with total disclinations that are multiples of +60°. The disclination of each structure corresponds to the presence of a given number of pentagons in the seed from which it grew: disks (no pentagons), five types of cones (one to five pentagons), of which only one was known previously[18], and open tubes (six pentagons). Statistical analysis of these domains shows some unexpected features, which suggest that entropy plays a dominant role in the formation of disclinations. Furthermore, the total disclination of a domain is determined mainly at the nucleation stage.

Several models have been proposed for the formation of fullerenes, which are also relevant to the nucleation of other curved structures such as nanotubes. The "pentagon-road"[1,3] and the "ring-stacking" models[4] are among the best known. The essence of the pentagon-road model is that small flat hexagonal networks of carbon have so much dangling-bond energy at the edges that, if the temperature and timescale are such as to permit annealing, the structures will try to eliminate dangling bonds by folding and incorporating pentagons until the structure is closed (12 pentagons or 4π total disclination). Dynamic calculations support this idea[5]. Reduction of the reaction enthalpy ΔH is the overriding concern in the pentagon-road model. In the ring-stacking model, it is proposed that curved surfaces are created by the selective assembly of monocyclic carbon rings[4], to account for the fact that only very few of the possible fullerene isomers are formed[15]. As it considers only certain reaction paths, the ring-stacking model is essentially driven by entropy changes (ΔS). Monocyclic rings are known to be the

dominant structures for cluster sizes between 10 and 30 carbon atoms, and some elegant experiments show that they can lead to the formation of fullerenes[9–11], although not necessarily in such a way as to support the ring-stacking model.

Although they start from very different considerations, both models contain as their key the probability of forming a disclination. However, we know next to nothing about the probability of forming curved carbon surfaces having disclinations consistent with one, two, three pentagons and so on. Furthermore, what does this probability tell us about the products and their yields?

Our sample was made by the pyrolysis of hydrocarbons in a carbon arc. We use an industrial-scale carbon-arc plasma generator (torch configuration) under a continuous flow of hydrocarbon (in this case heavy oil) at a typical feed rate of 50–150 kg h^{-1} and a reactor pressure of 2–3 bar. The solid carbon products are recovered and the residual undecomposed hydrocarbon and hydrogen are fed back into the reactor. The effective plasma temperature is hard to determine but from the level of graphitization of the sample, we estimate it to be at least 2,000 °C. The sample is composed nearly entirely of turbostratic (where the graphitic sheets are not ordered relative to each other in the plane) microstructures (Fig. 1) which have total disclinations (TD) that are a multiple of 60°: TD $= P \times 60°$, where $P \geqslant 0$, and corresponds to the effective number of pentagons necessary to produce that particular total disclination. Besides disks ($P = 0$), there are also a variety of cones. By considering the symmetry of a graphite sheet and Euler's theorem, it can be shown that only five types of cone can be made from a continuous sheet of graphite corresponding to values of P between 1 and 5. These are all present in this sample (Fig. 2a–e). The cone angle θ is given by $\sin(\theta/2) = 1 - (P/6)$. As far as we know, only the cone with TD $= 300°$ ($P = 5$) has been observed before[18]. Nanotubes are also present, although in smaller amounts. Figure 2f shows how the parallel basal planes follow the contour of the cone tip. Cones and nanotubes form ~20% of the sample, the rest being mainly disks.

We measured ~1,700 microstructures from transmission electron micrographs. The cone angle θ can be deduced from the projected dimensions of the tilted cones. A histogram of frequency versus cone angle θ (Fig. 3a) reveals that there are a number of maxima, which become better defined at smaller angles. Each maximum corresponds to a total disclination equivalent to between no pentagons and six pentagons. The width of the peaks increases with the cone angle θ mainly owing to measurement errors, it being hardest to accurately de-project the largest cone angles. In Fig. 3b the same data are reduced to the total count found at the average angle of each peak, with error bars, and corrected for underestimation of occurrence of cones with large angles. These angles correspond closely to those expected for solid angles which are multiples of 60° or an integer number of pentagons (open circles).

Figure 3 gives us the probability of nucleating each of type of microstructure and, therefore, of having seed structures with a given disclination (or number of pentagons). Surprisingly, there is a broad peak with a maximum at a cone angle corresponding to three pentagons. Reasoning on purely enthalpic grounds, one would have expected that small disclinations would have been more probable as they are less strained[19]. Thus, a Boltzmann distribution cannot account for the observed distribution as shown in Fig. 3b.

This result indicates that, whereas enthalpy (ΔH) is obviously the driving force for the formation of curved structures, entropy (ΔS) plays a dominating role in the distribution of disclinations formed. Here one must understand entropy changes in terms of the multitude of chemical pathways leading to a particular disclination. Furthermore, temperature will moderate the various possible pathways. A model like the ring-stacking model considers only a small subset of all the possible pathways leading to a given disclination. Monocyclic ring structures have been proved to favour the formation of fullerenes[9–11]. However, it is not clear if these monocyclic rings

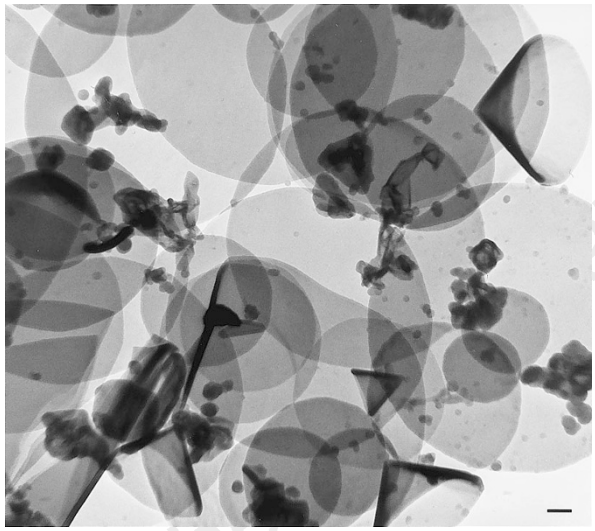

Figure 1 Transmission electron micrograph of the microstructures in the sample. Scale bar, 200 nm.

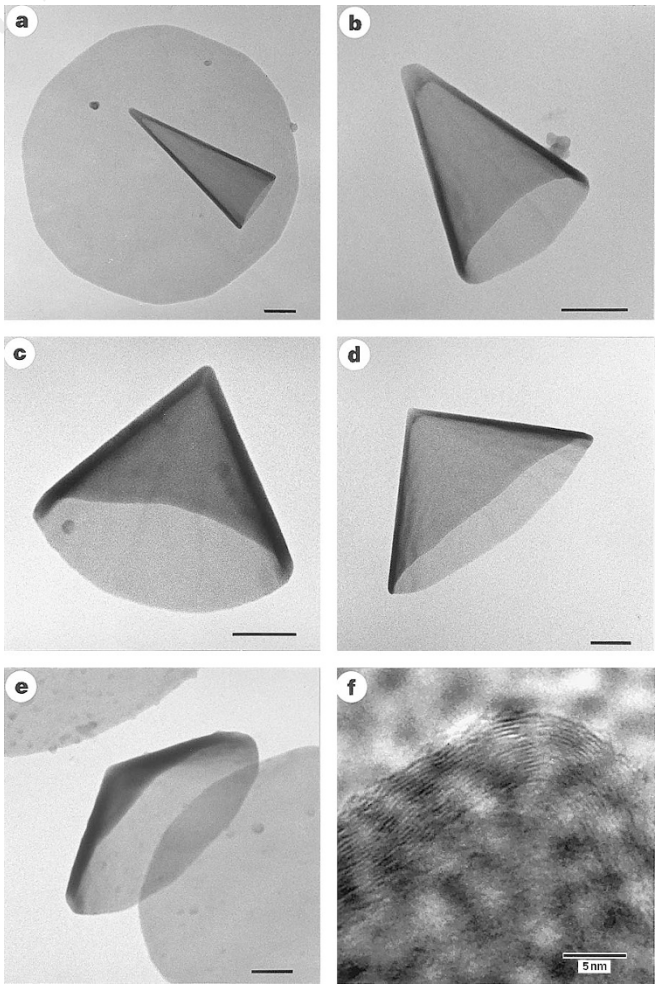

Figure 2 Examples of the five types of cones in the sample (scale bars in **a–e**, 200 nm): **a,** TD = 300°, θ = 19.2°; **b,** TD = 240°, θ = 38.9°; **c**, TD = 180°, θ = 60.0°; **d**, TD = 120°, θ = 84.6°; and **e**, TD = 60°, θ = 112.9°. Note the faceting of the disk in **a**. **f**, Higher magnification image of a cone tip (scale bar, 5 nm).

form the dominant pathway for the generation of all the disclinations observed in curved carbon structures. In principle, cones can be built by the growth of graphitic structures onto such rings. From statistical-mechanics considerations, there are many more ways of embedding a ring of a given size around the tip of a conical graphitic surface than into a graphite sheet. For example, there are 16 ways to embed a C_{16} ring into a planar graphite sheet about a fixed point, whereas there are 2,500 conformations of the same ring that will wrap around the tip of a $P = 2$ cone. Furthermore, starting from an odd-numbered open ring, a structure where P is even cannot be grown and vice versa, unless crosslinking of the ring occurs. Consequently, the pentagons are not the sole source of disclinations in the system. A disclination is inherent to the monocyclic ring topology and becomes fixed once growth has started. With monocyclic carbon seeds, pentagons are a consequence of the disclination, not vice versa. Of course, other seed topologies such as crosslinked rings will also be important. We are exploring this entropic "monocyclic avenue" further.

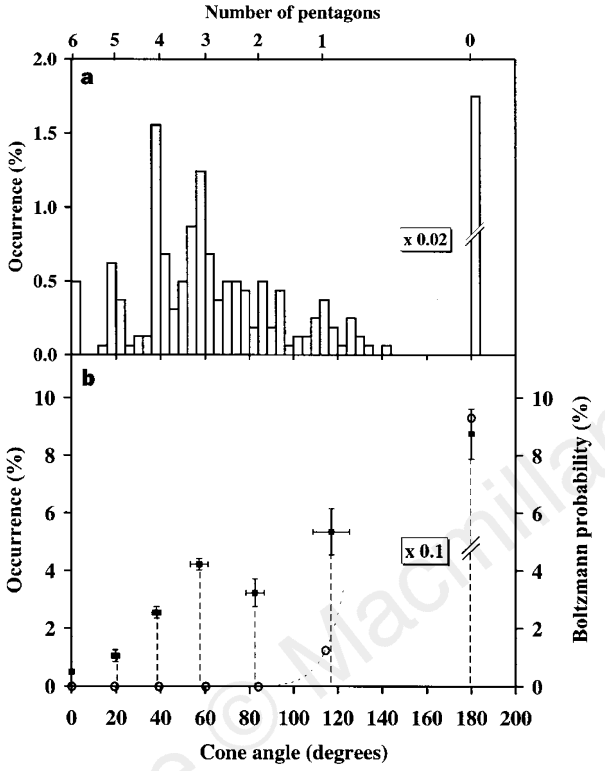

Figure 3 **a**, Statistical distribution of the measured cone angles among the microstructures; **b**, averaged distribution centred at the seven possible disclinations. The open circles and dotted line represent the calculated Boltzmann distribution of microstructures for a temperature of 2,000 °C and a pentagon energy of formation of 0.75 eV (ref. 19).

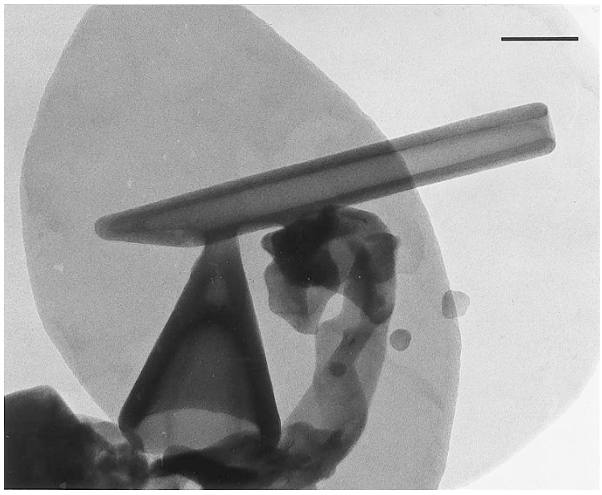

Figure 4 Example of tube formation after nucleation of a cone with a 300° disclination (scale bar, 200 nm). Note the open-ended growth.

Although a mixture of hydrocarbons was the source of carbon in these experiments, hydrocarbons are known to dehydrogenate at high temperatures[2], yielding under the right conditions the same family of products as a pure carbon plasma. Therefore, these findings should have broad implications for high-temperature generation of curved carbon structures. The wide distribution of disclinations, and the fact that this distribution is controlled by entropy, indicate that, in the absence of catalysts, it will always be hard to make a single type of disclination (except totally spheroidal structures) from a soup of carbon clusters, as discussed next.

Nanotubes and nanoparticles formed in a carbon arc have a bimodal distribution in terms of length[13,20]. Furthermore, yields of nanotubes versus nanoparticles have never been higher than about half the sample, despite numerous efforts over several years to increase the yields. Those results can now be better understood in the light of the distribution of seeds. At the higher temperature (3,700 °C) of formation of nanotubes in the arc, the probability of forming pentagons in a seed increases[6]. The optimal yield of nanotubes versus nanoparticles indicates that the distribution of seeds must be centred near six pentagons. However, all seeds with seven or more pentagons will inevitably form closed nanoparticles as the edges of the curved surfaces are on collision course as they grow. Seeds with six or fewer pentagons have a finite probability of becoming tubes, depending on the kinetics of growth and the probability of the introduction of another pentagon in the structure during the growth stage (see below). So what was originally a wide distribution of disclinations is now narrowed into mainly two products, hence the bimodal distribution[20]. The broad distribution of seeds also implies that it would be difficult to improve the yield of nanotubes beyond what has already been achieved. Conversely it is easy to reduce the yield of nanotubes by shifting the disclination maximum of the seeds, as found in nanotube fabrication.

The formation of spheroidal soot particles from hydrocarbons involves both nucleation and growth stages[16]. Although very little is known of the nucleation process[17], the possible connection to fullerene formation has been pointed out[1,2]. By analogy with colloidal suspensions, liquid hydrocarbon nuclei have been invoked to explain the formation of uniformly spherical soot particles[16]. In the context of these results, just like the nanoparticles, it suffices that the distribution of disclinations in the seeds is such that most of them have disclinations $>360°$ for all them to result in uniform spherical or polygonal particles. In other words, a broad distribution of disclinations in the seeds leads to nearly uniformly spheroidal soot particles.

Our results indicate that the total disclination, or curvature, is nearly always determined in the nucleation stage. A change in disclination after seeding (for example, the addition of pentagons or heptagons during growth) was rarely found in these samples. An example of such occurrence is shown in Fig. 4 where a cone with a 300° disclination has turned into a tube by the addition of a sixth pentagon. The relatively low probability of the formation of pentagons or heptagons during growth could point to different mechanisms of disclination formation in the nucleation and growth stages. Alternatively, it could be due simply to chemical factors during growth such as differences in rates or the thickening of structures. □

Received 21 April; accepted 17 June 1997.

1. Zhang, Q. L. *et al.* Reactivity of large carbon clusters: spheroidal carbon shells and their possible relevance to the formation and morphology of soot. *J. Phys. Chem.* **90,** 525–528 (1986).
2. Kroto, H. W. & McKay, K. The formation of quasi-icosahedral spiral shell carbon particles. *Nature* **331,** 328–331 (1988).

3. Smalley, R. E. Self-assembly of the fullerenes. *Acc. Chem. Res.* **25,** 98–105 (1992).
4. Wakabayashi, T. & Achiba, Y. A model for the C_{60} and C_{70} growth mechanism. *Chem. Phys. Lett.* **190,** 465–468 (1992).
5. Robertson, D. H., Brenner, D. W. & White, C. T. On the way to fullerenes: molecular dynamics study of the curling and closure of graphitic ribbons. *J. Phys. Chem.* **96,** 6133–6135 (1992).
6. Endo, M. & Kroto, H. W. Formation of carbon nanofibers. *J. Phys. Chem.* **96,** 6941–6944 (1992).
7. Iijima, S., Ajayan, P. M. & Ichihashi, T. Growth model for carbon nanotubes. *Phys. Rev. Lett.* **69,** 3100–3103 (1992).
8. Saito, Y., Yoshikawa, T., Inagaki, M., Tomita, M. & Hayashi, T. Growth and structure of graphitic tubules and polyhedral particles in arc-discharge. *Chem. Phys. Lett.* **204,** 277–282 (1993).
9. McElvany, S. W., Ross, M. M., Goroff, N.S. & Diederich, F. Cyclocarbon coalescence: mechanisms for tailor-made fullerene formation. *Science* **259,** 1594–1596 (1993).
10. von Helden, G., Gotts, N. G. & Bowers, M. T. Experimental evidence for the formation of fullerenes by collisional heating of carbon rings in the gas phase. *Nature* **363,** 60–63 (1993).
11. Hunter, J., Fye, J. & Jarrold, M. F. Carbon rings. *J. Phys. Chem.* **97,** 3460–3462 (1993).
12. Harris, P. J. F., Tsang, S. C., Claridge, J. B. & Green, M. L. H. High resolution microscopy studies of a microporous carbon produced by arc-evaporation. *J. Chem. Soc. Faraday Trans.* **90,** 2799–2802 (1994).
13. Gamaly, E. G. & Ebbesen, T. W. Mechanism of carbon nanotube formation in the arc discharge. *Phys. Rev. B* **52,** 2083–2089 (1995).
14. Charlier, J.-C., De Vita, A., Blase, X. & Car, R. Microscopic growth mechanisms for carbon nanotubes. *Science* **275,** 646–649 (1997).
15. Achiba, Y. *et al*. in *The Chemical Physics of Fullerenes 10 (and 5) Years Later* (ed. Andreoni, W. 139–47 (Kluwer Academic, Dordrecht, 1996).
16. Lahaye, J. & Prado, G. in *Particulate Carbon* (eds Siegla, D. C. & Smith, G.W.) 33–55 (Plenum, New York, 1981).
17. Harris, S. J. & Weiner, A. M. Chemical kinetics of soot particle growth. *Annu. Rev. Phys. Chem.* **36,** 31–52 (1985).
18. Ge, M. & Sattler, K. Observation of fullerene cones. *Chem. Phys. Lett.* **220,** 192–196 (1994).
19. Ihara, S., Itoh, S., Akagi, K., Tamura, R. & Tsukada, M. Structure of polygonal defects in graphitic carbon sheets. *Phys. Rev. B* **54,** 14713–14719 (1996).
20. Ebbesen, T. W. in *Carbon Nanotubes: Preparation and Properties* (ed. Ebbesen, T.W.) Ch. 4 (CRC, Boca Raton, 1997).

Acknowledgements. We thank M. E. Bisher for technical assistance.

Correspondence and requests for materials should be addressed to T.W.E.

Photoisomerization in dendrimers by harvesting of low-energy photons

Dong-Lin Jiang & Takuzo Aida

Fields and Reactions, Precursory Research for Embryonic Science and Technology, Japan Science and Technology Corporation, and Department of Chemistry and Biotechnology, Graduate School of Engineering, The University of Tokyo, Hongo, Bunkyo-ku, Tokyo 113, Japan

Infrared radiation can induce low-frequency molecular vibrations, but, with the exception of hydrogen-bond reorganization[1–3], the excitation energy tends to be dissipated rapidly through molecular collisions rather than inducing photochemical changes. Here we show that in a macromolecular system that is designed to be insulated against collisional energy scattering, infrared absorption can excite photoisomerization by multiphoton intramolecular energy transfer. We have prepared highly branched dendrimers[4–6] from aryl ethers with a photoisomerizable azobenzene core, in which infrared excitation of the aromatic units is apparently followed by a channelling of the absorbed energy to the core while the dendrimer matrix protects against collisional de-excitation. These findings suggest a strategy for harvesting low-energy photons to effect chemical transformations.

Dendrimers are nanometre-size macromolecules with a regular tree-like array of branch units[4–6]. We have recently synthesized dendrimer porphyrins in which a porphyrin chromophore is spatially isolated by the dendrimer framework[7–10]. As may be expected from the gradient in branch density from the interior to the exterior, the surface of these large dendrimers is conformationally frozen, whereas the interior space is not constrained irrespective of the size of the dendrimer framework, so that the core porphyrin is able to undergo free conformational motion[8]. Thus spherical, large dendrimers should provide a non-constrained environment insulated from collisional energy scattering. This motivated us to explore the possibility of intramolecular energy transfer within these unimolecular matrices.

For this purpose, we have synthesized a series of azobenzene-containing aryl ether dendrimers (*trans*-L*n*AZO, where *n* is the number of aromatic layers and is 1, 3, 4 or 5; Fig. 1), by alkaline-mediated coupling of dendritic benzyl bromides (L($n-1$)Br; ref. 8) with *trans*-3,3′,5,5′-tetrahydroxyazobenzene. We characterized this series of *trans*-L*n*AZO compounds unambiguously, by using ^{1}H NMR, ultraviolet–visible spectroscopy and matrix-assisted laser desorption ionization time-of-flight mass spectroscopy (further details are available; see Supplementary Information). Azobenzenes are photochromic molecules that isomerize from *trans* to *cis* on ultraviolet irradiation, and from *cis* to *trans* either thermally or on exposure to visible light[11]. Single-photon (ultraviolet) photoisomerization of azobenzene dendrimers similar to ours was demonstrated recently[12].

We measured ^{1}H NMR pulse relaxation times (T_1) of the *trans*-L*n*AZO family at 21 °C in $CDCl_3$, and confirmed an egg-like structural resemblance[8] to higher-generation *trans*-L*n*AZOs. The T_1 value for the methoxy protons on the exterior surface (filled circles in Fig. 2a) decreased sharply as the dendrimer framework became larger whereas that of the protons in the interior azobenzene functionality (open circles in Fig. 2a) remained almost intact. Thus L4AZO and L5AZO possess a non-constrained interior environment within a stiff exterior shell.

On ultraviolet radiation at 21 °C in $CHCl_3$, *trans*-L*n*AZO ($n = 1$, 3–5, 5×10^{-5} M) isomerized normally to *cis*-L*n*AZO, which then gradually isomerized back to the *trans* form after the irradiation was stopped. When a $CHCl_3$ solution of *cis*-L5AZO in a KBr cell was exposed to infrared radiation (a 75-W glowing nichrome source) in an infrared spectrophotometer, it isomerized very rapidly to *trans*-L5AZO. We found that this infrared-radiation-induced isomerization depends greatly on the size of the dendrimer framework (Fig. 2b): on exposure to the infrared radiation *cis*-L5AZO completely isomerized to the *trans* form in only 8 min (Fig. 3b) at a rate constant of 3.4×10^{-3} s^{-1}, which is 260 times as high as that of the thermal isomerization at 21 °C in the dark (1.3×10^{-5} s^{-1}, Fig. 2b) and even 23 times as high as the rate constant found on irradiation with visible light (440 ± 9 nm, 21 °C). Similarly, under infrared illumination *cis*-L4AZO underwent rapid isomerization to *trans*-L4AZO (Fig. 2b). In sharp contrast, we observed no effect of infrared radiation for the isomerization of the smaller homologues *cis*-L1AZO (Fig. 3a) and *cis*-L3AZO. *cis*-L1AZO was also unaffected by the infrared radiation even in the presence of a large dendritic benzyl alcohol (L5OH; 4 equiv.) unanchored to the azobenzene unit. Furthermore, although the molecular weight is almost comparable to that of L4AZO, the isomerization of *cis*-mono-L6′AZO (Fig. 1), a non-spherical mono-dendritic azobenzene, was not facilitated by infrared. Thus spatial isolation of the azobenzene functionality by the highly constrained, large dendrimer matrix (Fig. 2a) seems to be a prerequisite for the infrared-radiation-induced isomerization.

We further investigated the isomerization of *cis*-L5AZO (5×10^{-5} M, in $CHCl_3$ at 21 °C) by using monochromatized infrared radiation (a 75-W glowing nichrome source through a JASCO model CT-25C monochromator, bandwidth ±50 cm^{-1}) of three different wavenumbers; 2,500 cm^{-1} (transparent for L*n*AZO), 1,597 cm^{-1} (a stretching vibrational band for aromatic rings) and 1,155 cm^{-1} (a stretching vibrational band for CH_2–O), and found that only the 1,597 cm^{-1} radiation facilitates the isomerization reaction. This observation indicates that the infrared energy absorbed by the aromatic rings excites the *cis*-to-*trans* isomerization. We consider the following two possibilities for the mechanism of this effect; (1) direct infrared excitation of the interior azobenzene moiety, and (2) intramolecular energy transfer from the dendrimer matrix to the azobenzene. To investigate (2), we selectively excited the dendrimer framework of *cis*-L*n*AZO at its characteristic 280-nm absorption, where we again observed a definite